



UNIVERSITY OF LEEDS

This is a repository copy of *Novel ZnO-Ag/MWCNT nanocomposite for the photocatalytic degradation of phenol*.

White Rose Research Online URL for this paper:
<http://eprints.whiterose.ac.uk/133625/>

Version: Accepted Version

Article:

Hosseini, F, Kasaeian, A, Pourfayaz, F et al. (2 more authors) (2018) Novel ZnO-Ag/MWCNT nanocomposite for the photocatalytic degradation of phenol. *Materials Science in Semiconductor Processing*, 83. pp. 175-185. ISSN 1369-8001

<https://doi.org/10.1016/j.mssp.2018.04.042>

© 2018 Elsevier Ltd. This manuscript version is made available under the CC-BY-NC-ND 4.0 license <http://creativecommons.org/licenses/by-nc-nd/4.0/>.

Reuse

This article is distributed under the terms of the Creative Commons Attribution-NonCommercial-NoDerivs (CC BY-NC-ND) licence. This licence only allows you to download this work and share it with others as long as you credit the authors, but you can't change the article in any way or use it commercially. More information and the full terms of the licence here: <https://creativecommons.org/licenses/>

Takedown

If you consider content in White Rose Research Online to be in breach of UK law, please notify us by emailing eprints@whiterose.ac.uk including the URL of the record and the reason for the withdrawal request.



eprints@whiterose.ac.uk
<https://eprints.whiterose.ac.uk/>

Novel MWCNT/ZnO-Ag Nanoparticles for the Photocatalytic Degradation of Phenol

Farzaneh Hosseini¹, Alibakhsh Kasaeian², Fathollah Pourfayaz³, Mojgan Sheikhpour⁴, Dongsheng Wen^{5,6}

^{1,2,3} Department of Renewable Energies and Environment, Faculty of New Sciences and Technologies, University of Tehran, Tehran, Iran.

⁴ School of Biology, Faculty of Science, University of Tehran, Tehran, Iran.

⁵ School of Aeronautic Science and Engineering, Beihang University, Beijing, China

⁶ School of Chemical and Process Engineering, University of Leeds, Leeds, UK.

Corresponding Authors: Alibakhsh Kasaeian, akasa@ut.ac.ir, Tel: +98 9121947510

Dongsheng Wen, D.Wen@buaa.ac.uk,

Abstract:

A novel Ag-doped ZnO nanoparticle with different amounts of multi-walled carbon nanotubes (MWCNT) was developed in this work, aiming to shift the band edge toward longer wavelength, and provide more effective separation of electron/hole pairs. New particles were produced in a simple sol-gel method and assessed toward phenol degradation under UVA illumination. The photocatalysts were characterized by the X-ray diffraction (XRD), Raman spectroscopy, scanning electron microscopy (SEM) with an energy-dispersive X-ray (EDX) spectroscopy analysis, transition electron microscopy (TEM), BET surface area analyzer, UV-vis diffuse reflectance spectroscopy (DRS), and photoluminescence spectroscopy (PL). The results indicated that all the samples containing MWCNTs exhibited higher photocatalytic activity than bare ZnO and Ag-doped ZnO nanoparticles. At a 10% MWCNT addition, the novel particle achieved a photocatalytic conversion rate of 81% in removing 100 ppm phenol under UVA light after 240 min. The pH value, initial concentration and catalyst dosage were found to influence the particle's photocatalytic performance significantly, and the kinetics of phenol degradation followed the pseudo-first-order equation. The new particle could be utilized as a promising cost effective and environmentally friendly material for the degradation of organic pollutants.

Keywords: Multi-walled carbon nanotube; ZnO; photocatalyst; silver; phenol.

1. Introduction

Aromatic pollutants such as phenolic compounds are well known for their toxicity and non-biodegradable nature. These compounds are widely used in industries to produce petroleum products, pharmaceuticals, pesticides, paints and synthetic resins [1-3]. Because of their potential toxicity, many chemical and catalytic methods have been applied to decrease the concentration of aromatic pollutants to a safe level [4-6]. Since Fujishima and Honda[7] first reported photocatalysis by water splitting under UV irradiation, semi-conductor photocatalysts have been attracted extensive attention not only in water splitting but also for environmental remediation due to their non-toxic and environment-friendly nature, as well as low cost, high abundance, chemical and optical stability [3, 8-16]. The most commonly used photocatalytic semiconductors such as TiO_2 and ZnO have many limitations. For instance, ZnO nanoparticle has a wide band gap (3.37 eV) [16], and can only response to UV irradiation, which is a narrow spectral range of the total solar irradiation. High recombination rate of photo-generated electron-hole pairs is another limiting factor to achieve high photocatalytic efficiency. Hence, developing high visible-light-driven ZnO and enhancing the separation rate of electron-hole pairs are the main goals to improve the photocatalytic efficiency. To address these issues, a few methods have been proposed such as semiconductor combination [17-19], non-metal doping [20-23], transition and noble metal doping [24-28].

Noble metals such as Au, Pd and Ag have been shown to be effective on the enhancement of photocatalytic activity of ZnO nanoparticles [29-34]. Chen et al. synthesized Au-doped ZnO photocatalyst using hydrothermal and electrostatic self-assembly methods, which showed a higher photocatalytic activity due to more effective separation of charge carriers in the presence of Au [35]. Morales-Flores et al. studied the photodegradation of phenol with Pt-doped ZnO , which showed a highly active and selective catalytic performance, producing only one intermediate [36]. Whang et al. prepared Ag-doped ZnO via a laser-induction method to remove methylene blue under visible light irradiation and a higher efficiency was achieved with 2.0 wt% Ag at pH 11 after 8 hours [37]. Divband et al. revealed an important role of Ag doping on the charge separation and photocatalytic activity enhancement of ZnO particles [38]. Height et al. compared the performance of Ag- ZnO made from different methods on the photodegradation of methylene blue. The results showed that the Ag- ZnO catalysts synthesized via the flame spray pyrolysis method had more surface area than those

made from the wet-chemistry method, and yielded a better photocatalytic performance [39]. It has been reported that metal clusters on the surface of photocatalysts can reduce the charge carriers' recombination rate by trapping photo-induced electrons, resulting in an improvement of photocatalytic activity [39-43]. The large work function (4.26 eV) of Ag nanoparticles causes the formation of Schottky barrier at the metal-semiconductor interface [44].

Silver has been widely studied for p-type doping due to the high solubility, larger ionic size and minimum orbital energy [45]. Volnianska et al. reported that the ionization energy of Cu and Au were higher than Ag, which makes silver a good candidate for p-doping in ZnO [46]. Thomas et al. [47] reported that the substitution of Ag in ZnO lattice and the overlap of Ag 4d and O 2p states led to the formation of a new impurity band with lower Fermi level and induced p-type properties in ZnO. Generally, silver ions can occupy substitutional and interstitial sites in ZnO [48], however, Yan et al. [45] suggested that the formation energy of Ag at zinc substitutional sites was lower. Ag particles would generate intermediate energy states within the band gap of ZnO, which decreased the energy needed to transfer electron from the valance band to conduction band [49].

In recent years, many studies have shown that the photocatalytic performance of Ag/semiconductor nanostructures can be significantly improved in visible light region due to the localized surface plasmon resonance (LSPR) properties of Ag nanoparticles [50-54]. For instance, Khademalrasool et al. [55] attributed the enhancement of photocatalytic activity to the energy transfer from Ag nanowires to ZnO nanoparticles due to Ag's LSPR effect. Liu et al. [51] suggested that the synergistic effect of mesoporous structures of some metal oxide semiconductors and plasmonic enhanced light absorption of Ag nanoparticles could result in highly active photocatalysts.

Recently, there has been extensive interest in the use of carbon-based nano materials as a catalyst support. Carbon nanotube (CNT) is a candidate due to its high aspect ratio, large surface area, high electron mobility and phenomenal flexibility [56]. According to the conduction band (CB) and valance band (VB) of ZnO (i.e., -4.05 and -7.25 eV in vacuum) [57] and the work function of CNTs (i.e., -4.5 eV in vacuum)[58], under UV light irradiation, the electrons would be excited from VB of ZnO to CB, which is then then transferred to CNTs. CNTs can act as both electron-acceptor and electron-transport materials to reduce the charge carrier recombination, hence improving the photocatalytic efficiency [59-61]. Multi-

walled CNT (MWCNTs) are great adsorbent with high surface area with many active sites for photocatalytic degradation of pollutants. CNT also plays an important role as a dispersing agent, influencing the morphology and particle size of ZnO [62]. Martinez et al. investigated the photocatalytic degradation of Carbamazepine (CBZ), 5H-dibenzo[b,f]azepine-5-carboxamide under near UV irradiation using TiO₂, ZnO and MWCNT [63]. Jiang and Gao fabricated ZnO coated MWCNTs composite using noncovalent modification of MWCNTs with a dispersant sodium dodecyl sulfate (SDS). This composite exhibited a higher photocatalytic activity than pure ZnO and mechanical mixed MWCNTs and ZnO [64]. Bu synthesized MWCNT/ZnO:Al:N nanocomposite film via a sol-gel deposition method, a higher photocatalytic efficiency in the degradation of methylene blue was observed[65]. Byrappa et al. fabricated ZnO:CNT and TiO₂:CNT composites under hydrothermal conditions, and both composites showed higher photocatalytic performance than those from pure ZnO, TiO₂ and hydrothermally prepared ZnO:AC and TiO₂:AC composites [62].

Utilizing the unique properties of Ag and CNT, this work proposed a novel catalytic particle concept, i.e., Ag-doped ZnO nanoparticle on the support of MWCNTs. It was expected that Ag doping would cause a band edge shift toward longer wavelength, and the incorporation of MWCNTs would enhance the visible light absorbance and effective separation of electron/hole pairs, leading to more efficient photocatalytic effect. These novel particles were produced in a simple sol-gel method, and a parametric study of the effects of the catalyst concentration, solution pH and the initial concentration of pollutant were investigated on the photocatalytic degradation of phenol. The new particle could be utilized as a promising cost effective and environmentally friendly material for the degradation of organic pollutants.

2. Materials & Methods

2.1. Materials

High purity MWCNTs were obtained from Research Institute of Petroleum Industry. Further purification of the MWCNTs was accomplished by ultra-sonication in concentrated nitric acid at 70°C for 6h, followed by centrifuging and washing with distilled water, then drying at 100 °C overnight in oven.

Other chemical reagents such as zinc acetate ($\text{Zn}(\text{OAc})_2 \cdot 2\text{H}_2\text{O}$), silver nitrate (AgNO_3), sodium hydroxide (NaOH), Sulfuric Acid (H_2SO_4), hydrochloric acid (HCl), nitric acid (HNO_3) and phenol were obtained from Merck Company and were used as received without further purification. All solutions were prepared using deionized water as solvent.

2.2. Preparation of photocatalyst and pollutant

- Preparation of MWCNT/ZnO-Ag

To prepare MWCNT/ZnO-Ag nanoparticles, a 0.1 M zinc acetate solution with small amount of silver nitrate (0.001M) was prepared in 100 ml of deionized water. Then various concentrations of MWCNTs (i.e., $x = 0.022, 0.11, 0.22$ and 0.44 gr, equivalently 1%, 5% , 10% and 20% MWCNT in mass, respectively) were introduced into the solution. After ultrasonic dispersion for 30 min, sodium hydroxide solution was added drop-wise into the obtained solution until reaching pH 7 under continuous stirring. Afterwards, the products were aged at room temperature for 12 h, separated centrifugally, washed several times with distilled water and dried at 70°C for 6 h in an oven. Finally, the resulting powder was calcined at 400°C for 2 h in an electrical furnace at a temperature increase rate of 3°C min^{-1} . For comparison, ZnO and ZnO-Ag nanoparticles were also prepared by the above-mentioned method without MWCNTs or Ag under the same conditions.

- Preparation of pollutant

To prepare synthetic wastewater, specific amount of phenol was dissolved in 300 ml of deionized water to obtain a 100 ppm solution for each photocatalytic run.

2.3. Test of photocatalytic activity

The photocatalytic activity was evaluated by the degradation of phenol in a 300 ml aqueous solution containing 0.3 g of photocatalysts and a phenol concentration of 100 mg/L at inherent pH (6.8) of solution. To reach adsorption-desorption equilibrium, the suspension were agitated in dark for 60 min. After that, the concentration of phenol was recorded as C_0 and then experiments were carried out further for 240 min under UVA light irradiation. After every 30 min, 3 ml suspension was sampled and centrifuged (4000 rpm for 3 min) immediately. The residual concentration (C) of phenol was evaluated using a UV-vis spectrophotometer (nanodrop2000) and a calibration curve. To investigate pH effect on photocatalytic degradation of phenol, pH was adjusted using diluted HCl or NaOH solution.

In order to investigate the reusability of ZnO-Ag-MWCNTs, the used photocatalysts were separated centrifugally, washed with distilled water for five times, dried at 70 °C for 6h and then used in 10 cycles with the same operational condition.

2.4. Set-up and experimental data gathering

Fig.1 shows a schematic diagram and the experimental setup used to evaluate the photocatalytic performance of the synthesized photocatalysts. All photocatalytic experiments were conducted in a batch mode. The cylindrical glass photo-reactor consisted of an outer Pyrex cylinder with 6 cm diameter and 30 cm long, and an inner quartz tube with 2.5 cm diameter and 35 cm long, which could be fitted with a cylindrical UV lamp. An 8 W Osram UVA lamp with an emission range between 300 to 400 nm were located in the center of photo-reactor as the source of light. An air pump, air distributors and magnetic stirrer were used to agitate the suspension during the experiments. To prevent UV exposure, the photo-reactor was covered with aluminum foil.

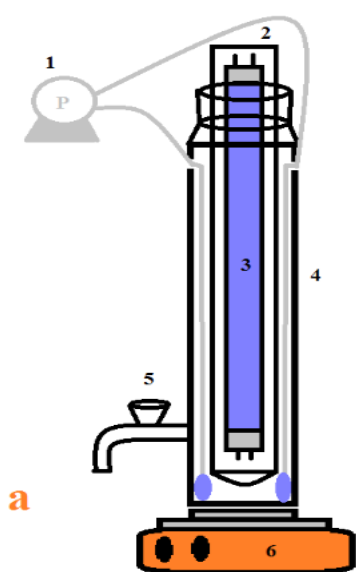


Figure 1. a: Schematic diagram of the experimental setup, (1) Air pump, (2) Inner quartz tube, (3) UVA lamp, (4) Pyrex reactor, (5) Sampling valve, (6) Stirrer – b: experimental setup.

2.5. Characterization

The crystal structure and phase purity of nanocomposite were characterized by X-ray diffraction analysis (XRD, Siemens D500) at room temperature using Cu K α radiation ($\lambda=1.540 \text{ \AA}$) in the 2θ range of $20\text{-}80^\circ$. The specific surface area was calculated using Brunauer Emmett Teller surface area analyzer (BET) from the measurements of N₂-adsorption at 77 k. The surface morphology and particles size of nanoparticles were examined using a scanning electron microscope (SEM, Zeiss DSM-960A) and transmission electron microscope (TEM, Philips CM120). The surface elemental compositions of the prepared photocatalysts were investigated by energy dispersive X-ray spectroscopy (EDS, attached to SEM). The band gap and optical properties of the samples were identified using UV-visible diffuse reflectance spectra (UV-vis-DRS, Avantes, Avaspec-2048TEC) and Photo-luminescence emission spectra (PL, Avantes, Avaspec-2048TEC). The sample was excited with a 325 nm wavelength light at room temperature and the emission scanned between 300 and 700 nm. Raman spectra were recorded using a Teksan-TekramP50C0R10 with 532 nm wavelength incident laser light.

3. Result and discussion

3.1. XRD analysis

The crystalline structure of samples was studied using XRD analysis. Fig. 2 shows the XRD patterns of as-prepared nanoparticles. The diffraction peaks at 2θ of 31.73, 34.25, 36.14, 47.48, 56.58, 62.6, 67.64, 68.81 and 72.32 are respectively assigned to (100), (002), (101), (102), (110), (103), (112), (201) and (004) diffraction planes of hexagonal Wurtzite ZnO (JCPDS NO 36-1451).

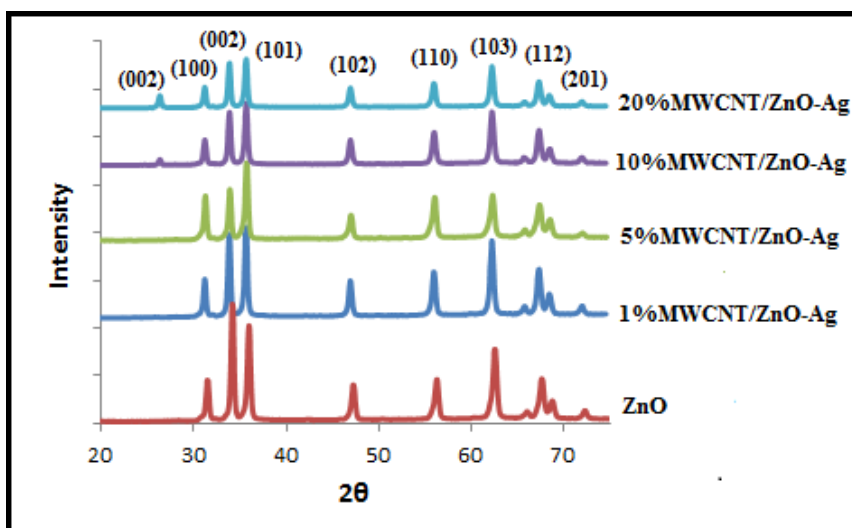


Figure 2. XRD diffractogram

The XRD pattern of 20% MWCNTs/ZnO-Ag sample reveals a weak peak at $2\theta = 26.3$, which is generally attributed to the (002) diffraction plane of MWCNTs. This peak is not detected in other MWCNTs/ZnO-Ag samples due to the low content and the low diffraction intensity of MWCNTs compared to ZnO. There is no characteristic peak of Ag in XRD patterns, which is ascribed to low amount of Ag. No other diffraction peaks are distinguished, showing the nanoparticles were successfully synthesized without any impurity phases. It should be noted that all diffraction peaks of ZnO in Ag doped samples were slightly shifted to the lower angles, indicating the incorporation of Ag atoms into ZnO sites. The ionic size difference between Ag (0.126 nm) and Zn (0.074 nm) leads to an expansion of ZnO lattice and an increase of lattice parameters.

3.2. SEM and TEM

The morphology and size of the sample were characterized by SEM analysis. Figure 3 shows the SEM images of the prepared samples with different MWCNTs contents. The as-synthesized samples were found to be almost spherical in shape. In different samples the average particle size was measured from 40 nm to 100 nm.

The SEM images of 1%, 5% and 10% MWCNT-ZnO-Ag samples show that all of the MWCNTs are covered with a dense layer of ZnO nanoparticles. It can be clearly seen that ZnO nanoparticles grow into the interspaces of CNTs. The ZnO nanoparticles dispersed on CNTs surface confirm a strong interaction and binding between CNTs and ZnO nanoparticles. As shown in Fig. 3 d,e, a further increase of MWCNTs content results in their

appearance in SEM images. For 20% MWCNTs- ZnO- Ag sample, CNTs act as substrates for growth of nanoparticles. It has been reported that the introduction of an optimal amount of CNTs prevents ZnO particles from agglomeration and growth, resulting in the increase of surface area.

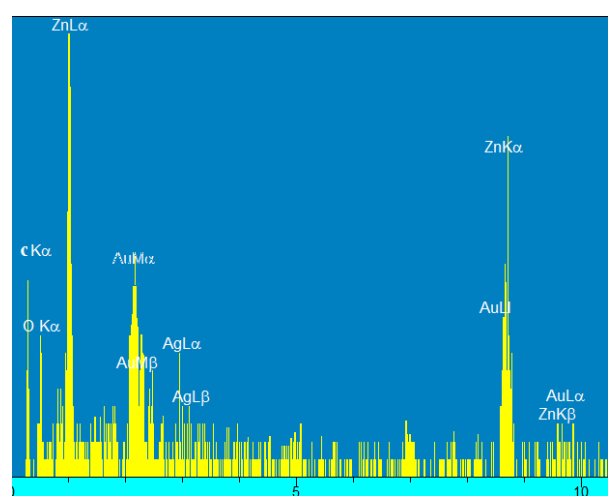
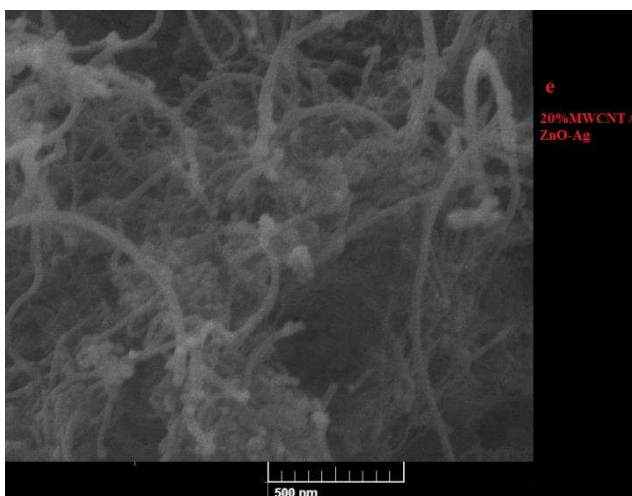
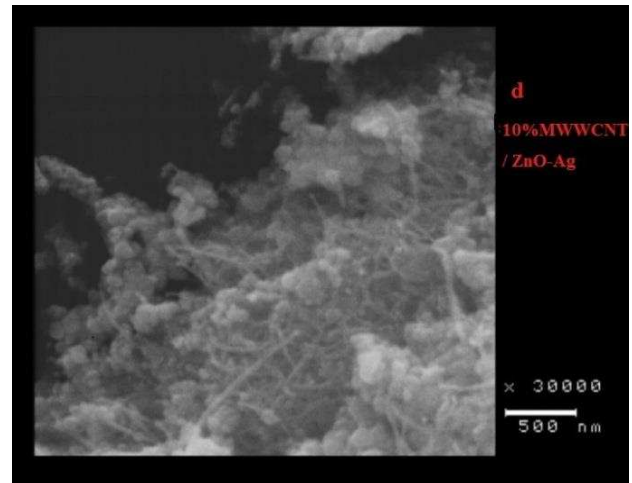
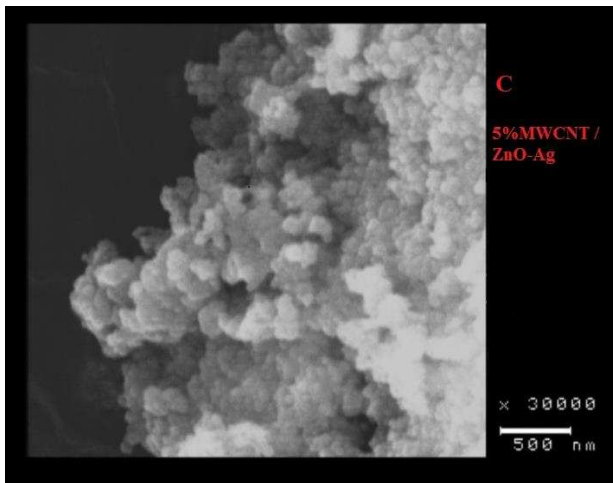
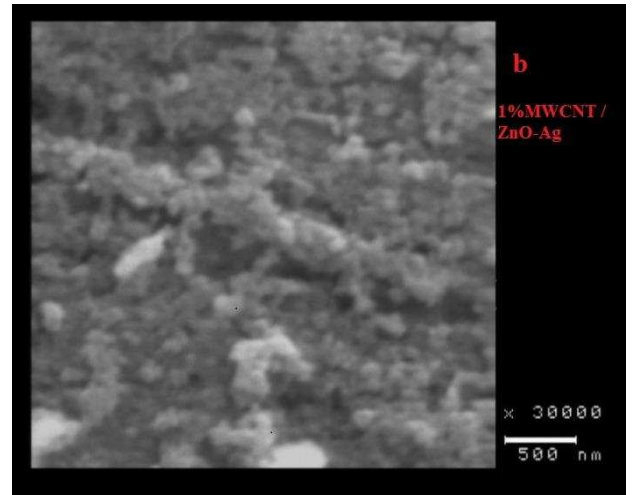
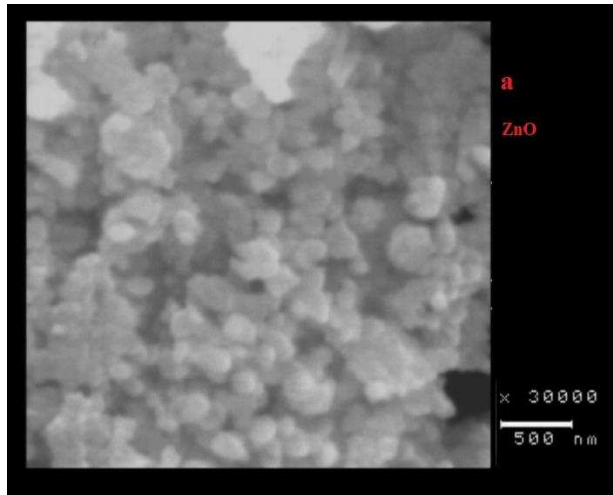


Figure 3. SEM image of ZnO (a), 1% MWCNT/ZnO-Ag (b), 5% MWCNT/ZnO-Ag (c), 10% MWCNT/ZnO-Ag (d), 20% MWCNT/ZnO-Ag (e), EDS analysis of 20% MWCNT/ZnO-Ag (f)

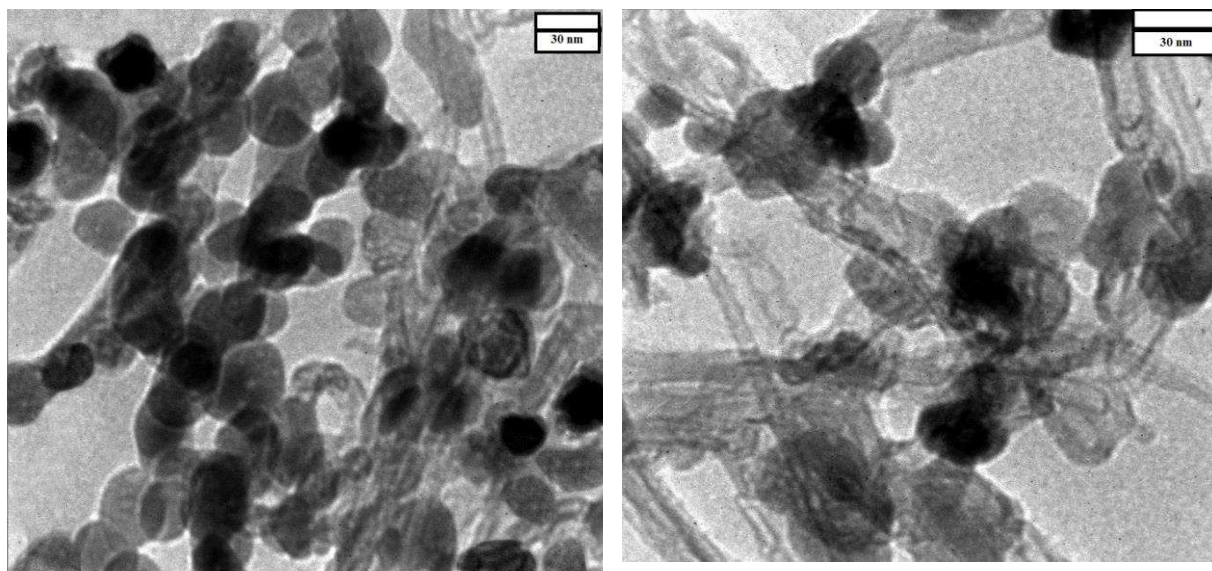


Figure 4. TEM images of 10% MWCNT/ZnO-Ag (a), 20% MWCNT/ZnO-Ag (b).

EDX was carried out to probe the composition of nanoparticles. Figure 3e reveals the presence of Zn, O, C and Ag on the surface of nanoparticles, which confirms the existence of ZnO-Ag nanoparticles on MWCNTs. It is estimated that there is 1.68 at% of Ag in ZnO.

The morphologies of 10% and 20% MWCNT-ZnO-Ag nanoparticles were further investigated using TEM. The TEM image of 10%MWCNT-ZnO-Ag clearly shows that the particles are dispersed homogeneously, and all of the MWCNTs are covered with ZnO nanoparticles (Fig. 4). The approximate sizes of particles are between 30 and 40 nm. The TEM image of 20%MWCNT-ZnO-Ag exhibits individual CNTs, which are not covered with ZnO particles. The size of particles has not considerably changed in comparison to 10%MWCNT-ZnO-Ag particles.

3.3. BET

The BET surface areas and pore structures of synthesized samples were investigated using nitrogen adsorption- desorption isotherms and BJH pore size distribution. The results are summarized in Table 1. The BET surface areas increased significantly with increasing the

CNT, range from 7.38 m²/g to 109.7 m²/g for ZnO and 20% MWCNT/ZnO-Ag samples, respectively. The larger specific surface area of MWCNT/ZnO-Ag nanoparticles is associated to its ability to transfer charge carrier, resulting in enhancing photocatalytic activity.

Table 1. Texture properties of the samples

Sample	BET Surface Area (m²/g)	Pore Volume (cm³/g)	Pore Size (nm)
MWCNT	207.96	0.5648	11.97
ZnO	7.39	0.0297	37.04
1%MWCNT/ZnO-Ag	8.52	0.0401	30.98
5%MWCNT/ZnO-Ag	10.37	0.0421	27.83
10%MWCNT/ZnO-Ag	17.81	0.0477	13.37
20%MWCNT/ZnO-Ag	109.7	0.24	11.35

Figure 5 shows the N₂ adsorption-desorption isotherms for MWCNTs and 10% MWCNT/ZnO-Ag samples. The isotherms are type IV with a H₃ type hysteresis loop according to the Brunauer- Dening- Teller classification, indicating a mesoporous material with slit-shaped pores. The isotherms don't show any limiting adsorption at high P/P₀. The Barrett-Joyner-Halenda (BJH) pore sizes determined from adsorption branches are changed from 37.04 nm for ZnO to 11.35 nm for 20%MWCNT/ZnO-Ag. The pore size distribution of samples varied from 2 to 100 nm, suggesting the formation of large mesopores and macropores.

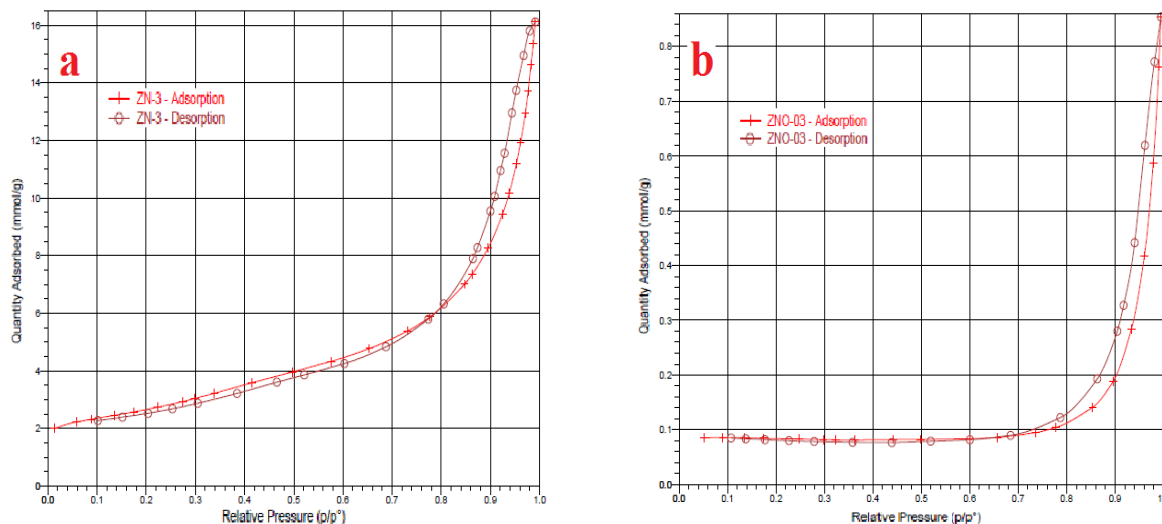


Figure 5. adsorption- desorption isotherms at 77 k of pure MWCNT (a) and 10%MWCNNT/ZnO-Ag (b)

3.4. Raman

The Raman spectroscopy analysis has been applied to study functionalized MWCNT and 10%MWCNT/ZnO-Ag and confirm the presence of MWCNT in the synthesized sample. As shown in Fig. 6, the Raman spectra shows a D band at about 1350 cm^{-1} for functionalized MWCNT and at 1339 cm^{-1} for 10% MWCNT/ZnO-Ag. This band is known as the disordered or defect mode and is caused by disorder in sp^2 hybridized carbon system. In addition, a signal of G band appears at 1582 cm^{-1} for functionalized MWCNT and at 1571 cm^{-1} for 10%MWCNT/ZnO-Ag that is due to the E_{2g} vibrational mode, arising from the stretching of C-C bond in graphitic materials. The peaks at 2710 cm^{-1} for functionalized MWCNT and at 2675 cm^{-1} for 10%MWCNT/ZnO-Ag are known as 2D band, associating with the splitting of electron bands.

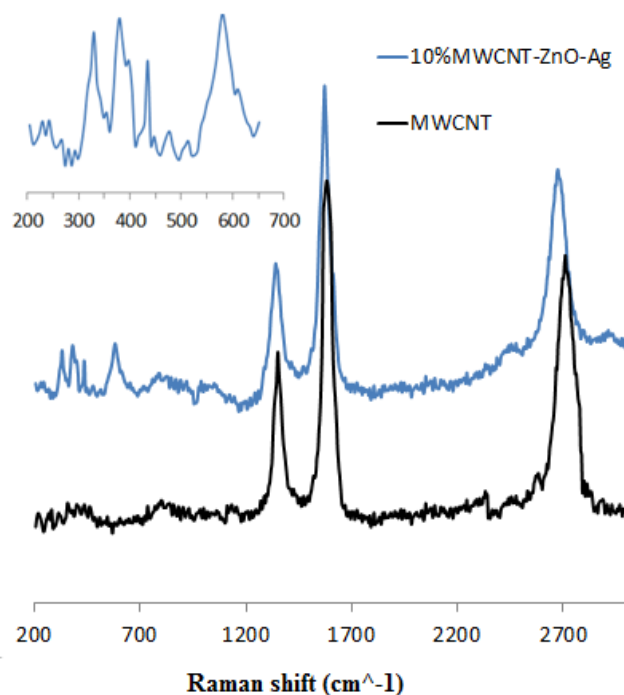


Figure 6. Raman spectrum of MWCNT and 10%MWCNT/ZnO-Ag

Four other peaks at 330, 379, 434 and 579 cm^{-1} for 10%MWCNT/ZnO-Ag sample correspond to presence of ZnO nanoparticles. A slight shift of peaks position can be attributed to the formation of new bonds between MWCNT and ZnO due to carbon substitution in ZnO lattice. The intensity ratio of the D band to the G band (I_D/I_G) is considered for evaluating the structure changes of carbon materials and the degree of disorder in MWCNTs walls. The intensities ratio decreases from 0.59 for MWCNT to 0.54 for 10%MWCNT/ZnO-Ag, indicating lower defects and disorders for 10%MWCNT/ZnO-Ag sample.

3.5. DRS

High optical absorbance in a wide range of solar spectrum is essential for effective photocatalysis. Figure 7 (a) shows the UV-vis absorbance spectra of the ZnO nanoparticles with and without MWCNT-Ag composites in the range of 300–700 nm. As shown in Fig. 7, the UV absorptions of all MWCNT/ZnO-Ag samples are higher than ZnO nanoparticles and the introduction of Ag and MWCNT have an impressive effect on UV light absorption. Moreover, the absorbance in visible region increases significantly with increasing MWCNT content, which is compatible with the samples' color, changing from white for ZnO to black

for 20%MWCNT-ZnO-Ag sample. Among them, the 20%MWCNT-ZnO-Ag sample has the highest absorbance in the visible region. It may happen because the porous structure of MWCNT-ZnO-Ag, which can trap and scatter the light inside and make the light path longer. This enhancement in light absorbance plays an important role in determining the performance of photocatalyst. The shift of absorption edge toward visible region in MWCNT-ZnO-Ag samples can be attributed to the change of band gap energy caused by Ag doping. There is not much change in the absorption edge with increasing MWCNTs content.

The optical band gap energy of samples was calculated from UV-vis DRS spectra and the Tauc method:

$$\alpha \cdot h\nu = k(h\nu - E_g)^{n/2} \quad (1)$$

where α is absorption coefficient, k is constant, h is the Planck's constant, ν is light frequency, $n=1$ for direct electronic transition, $n=4$ for indirect electron transition and E_g is the energy gap. As shown in Fig. 7 (b), the band gap energy of the Ag-doped ZnO decreases comparing to un-doped ZnO. The increase of MWCNT content doesn't have remarkable effect on the Band gap energy as ZnO and MWCNT are in two different phases. The reduction in band gap of MWCNT-ZnO-Ag samples is mainly attributed to the presence of the p-type conductivity in the silver-doped ZnO nanoparticles. These results agree with data reported elsewhere.

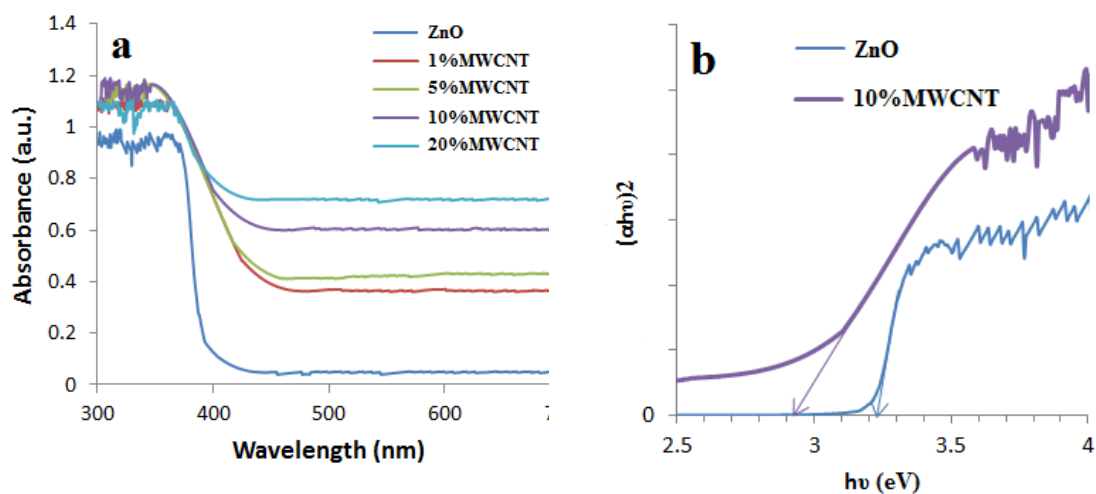


Figure 7. The UV-vis diffuse reflectance spectra (DRS) of samples (a), Tauc plot for ZnO and 10% MWCNT/ZnO-Ag (b).

3.6. Photoluminescence test

Figure 8 shows the room temperature photoluminescence (PL) emission measurement (excitation at 325 nm) of synthesized samples. The spectra of as-prepared ZnO exhibited both UV and VIS emission peaks centered at 390 nm and 600 nm. The two PL emission peaks of high quality ZnO have been reported at 380 nm (near band emission) and 550 nm (green) in many articles. The near band emission peak is attributed to the luminescence from localized surface states due to the recombination of free excitons, and the green emission is ascribed to defects such as zinc interstitials and oxygen vacancies in ZnO. The PL intensity is associated with the relative rate of recombination. As shown in Fig. 8, ZnO sample has the highest intensity and the PL intensity decreases with increasing CNTs content, implying a reduced recombination of electrons and holes with the incorporation of CNTs. Since ZnO is a good electron donor and carbon materials are good electron acceptors, the introduction of MWCNTs to the nanoparticles leads to electron transfer from ZnO conduction band to new energy levels of MWCNTs, resulting in the retardation of charge carriers recombination and enhancement of photocatalytic activity.

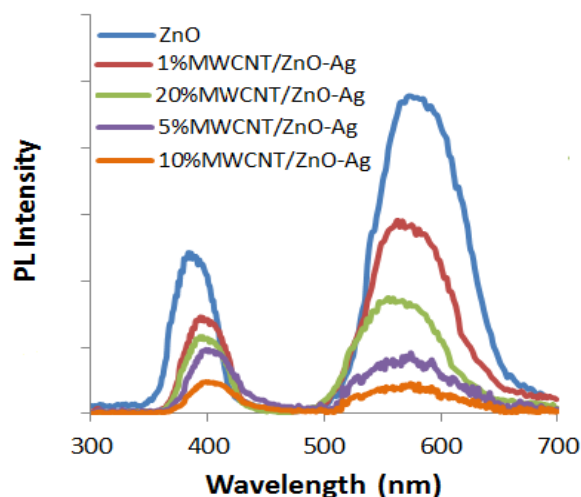


Figure 8. Photoluminescence (PL) spectra of samples

On the other hand, the conduction band of ZnO is higher than the new equilibrium Fermi energy level of Ag/ZnO, which facilitates the transfer of photo-excited electrons from

conduction band of ZnO to Ag nanoparticles. It seems that the doping of Ag and addition of CNTs result in a strong shift of emission peaks due to defects creation.

3.7. Photocatalytic experiments

- Photocatalytic activity of the as-synthesized samples under UVA light illumination:

Figure 9 shows the photocatalytic performance of six synthesized samples (1 g/L) by the degradation of phenol ($C_0= 100$ ppm) under UV irradiation. No activity was observed in the absence of catalyst or light irradiation or over the bare MWCNTs. As shown in Fig. 9, ZnO nanoparticles can only reach 49% of phenol removal after 240 minutes radiation. However, 81% of removal was achieved for 10%MWCNT/ZnO-Ag sample within the same reaction time. The ZnO sample shows the least photocatalytic activity due to the wide band gap and high recombination rate of charge carriers, which limits its photocatalytic application under UV and visible light irradiation.

After successful incorporation of MWCNT and Ag, the samples have shown to be more effective in the degradation of phenol. The Ag doping leads to a narrower band gap energy, besides that, the introduction of optimum MWCNTs suppresses effectively the recombination of electron and hole pairs by trapping electrons (as confirmed by PL analysis), and enhancing the light harvesting in both UV and visible region, which is favorable to the photocatalytic activity of nanoparticles. On the other hand, as the BET analysis demonstrated, the specific surface area of the hybrid particle is increased with increasing MWCNTs content. Thus the samples with more MWCNTs can provide more active sites to adsorb phenol, leading to improved photocatalytic degradation. In the presence of Ag and MWCNTs, more reactive oxidative species such as hydroxyl radicals ($\bullet\text{OH}$) can be created, resulting in better photocatalytic activity. Moreover, the oxygen provided by the air pump adsorbs on the surface of photocatalysts and traps the conduction band electrons with the formation of superoxide radical ions ($\text{O}_2^{\bullet -}$). Since the transfer of photo-generated electrons from ZnO particles to the MWCNTs occurs across the interface between ZnO and MWCNTs, the degree of interfacial contact plays a key role on the charge carrier transfer. It has been reported that the size of ZnO particles could affect the synergetic interaction between ZnO and MWCNTs. The smaller particle size of 10%MWCNT-ZnO-Ag nanoparticles, as shown in SEM pictures, could be another reason for its higher photocatalytic activity.

The lower photocatalytic efficiency for 20%MWCNT/ZnO-Ag in comparison to 5% and 10% MWCNT/ZnO-Ag can be attributed to the higher rate of recombination of photo excited

electron/hole pairs, which was confirmed by PL analysis. The MWCNTs incorporation beyond the optimum amount would produce more recombination centers, leading to the reduction of photocatalytic performance. Furthermore, SEM images revealed less effective interaction between ZnO and MWCNTs and more non-uniform dispersion of ZnO nanoparticles on CNTs for 20%MWCNT/ZnO-Ag sample in comparison to 5% and 10% MWCNT/ZnO-Ag samples.

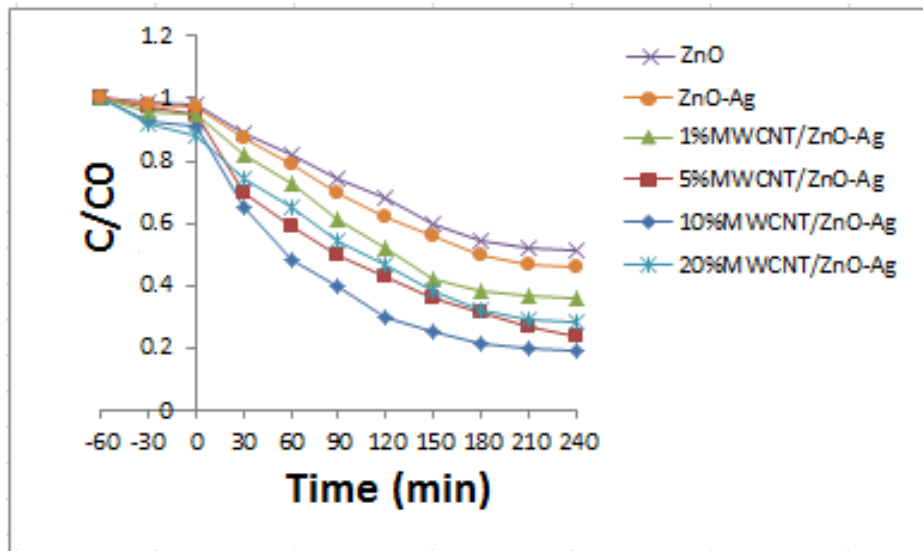


Figure 9. Photocatalytic degradation of phenol using different samples ($C_i = 100$ ppm, photocatalyst dosage = 1 g/L, pH = 6.8)

- Effect of pH

The pH of the aqueous solution influences the surface charge on the semiconductor particles, pollutant dissociation and adsorption, the aggregate formation and oxidation potential of the valance band. A series of experiments were conducted at initial pH of 3, 5, 9 and 6.8 as the inherent pH of phenol solution. All the experiments were carried out under UV light irradiation using 1 gr/L of 10%MWCNT-ZnO-Ag photocatalyst in 300 ml of solution with phenol concentration of 100 ppm. The degradation percent of phenol after 240 min irradiation was 42%, 78%, 81% and 53% at pH 3, 5, 6.8 and 11, respectively.

To explain the influence of pH, the properties of both phenol and photocatalyst particles should be taken into consideration. It is known that the surface of photocatalyst is positively charged at a pH lower than the point of zero charge (pzc) and negatively charged at a pH

higher than pzc. It has been reported that the zero point charge for ZnO is 9.0, above this value ZnO^- is predominantly formed and at pH below the pH_{zpc} , the ZnO surface is protonated to form ZnOH^{2+} . Therefore, 10%MWCNT-ZnO-Ag was positively charged at pH 3, 5 and 6.8, while negatively charged at pH 11. On the other hand, phenol is a weak acid with a pK_a value of 9.89. It means that for pH below this value, the phenol is appeared in molecular form, whereas for pH value above that, the aromatic ring becomes negatively charged by means of the hydroxyl group ionization. Thus, in pH 11 both phenol and 10%MWCNT-ZnO-Ag nanoparticles acquire negative charge, and the electrostatic repulsion retards the phenol adsorption. In addition, the competitive adsorption of ions from NaOH could also decrease phenol adsorption and degradation efficiency. In pH 6.8 and 5, molecular form of phenol can easily attach to the positive surface of photocatalysts and enhance the degradation efficiency. The lower photocatalytic efficiency in strong acidic media (pH=3) could be ascribed to the extreme adsorption of Cl^- ions on ZnO surface and also the corrosion of photocatalyst surface.

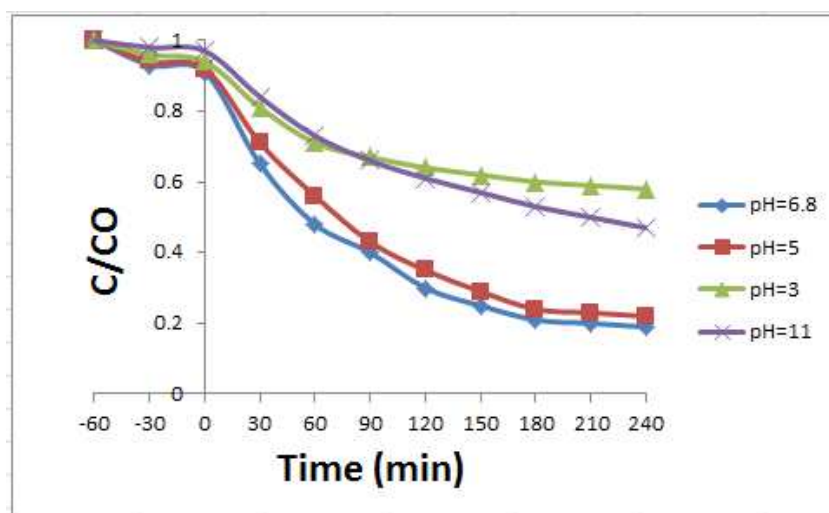


Figure 10. photocatalytic degradation of phenol using 10%MWCNT/ZnO-Ag ($C_i=100$ ppm, photocatalyst dosage= 1 gr/L)

- Effect of catalyst dosage

To investigate the effect of photocatalyst dosage, a series of experiments were carried out in the presence of 0.5, 1 and 1.5 gr/L 10%MWCNT-ZnO-Ag photocatalyst, under UV light irradiation for 240 min with initial pH and phenol concentration of 6.8 and 100 ppm,

respectively. As shown in Fig. 11, the efficiency of phenol degradation was higher at the photocatalyst dosage of 1 gr/L. The increase of photocatalyst concentration to the optimum dosage provides more adsorption sites and effective light absorption to generate electron and hole pairs, resulting in an enhancement of photocatalytic degradation. The excessive amount of photocatalysts may darken the solution, increase the light scattering and consequently, decrease the generation of electron and hole pairs. On the other hand, any further increase in catalyst concentration beyond the optimum value leads to the aggregation of photocatalyst particles, causing a decrease in the number of active sites and pollutant adsorption.

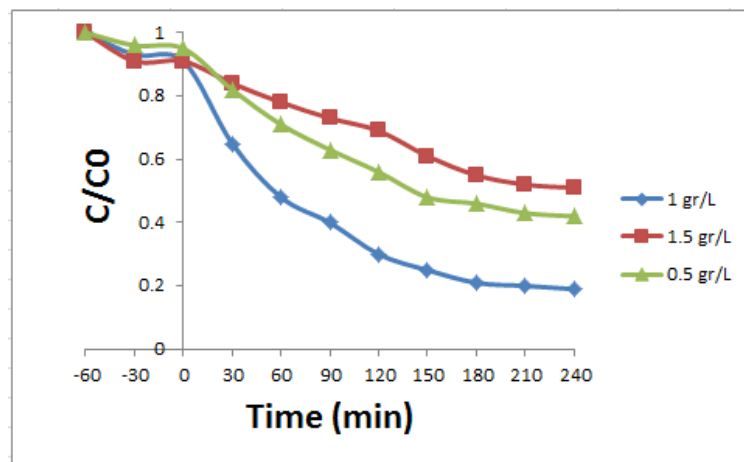


Figure 11. Photocatalytic degradation of phenol using 10%MWCNT/ZnO-Ag ($C_i=100$ ppm, pH=6.8)

- Effect of initial phenol concentration

As shown in Fig. 12, the effect of different initial phenol concentrations (25, 50, 100 and 150 ppm) on the photocatalytic degradation efficiency were evaluated under UV light irradiation at the initial pH of 6.8 and 10%MWCNT-ZnO-Ag dosage of 1 g/L. The degradation efficiency decreases significantly with the increase of the initial phenol concentration. The maximum efficiency was achieved at a phenol concentration of 25 ppm. It could be attributed to the excessive phenol molecules in the solution, which occupy active sites of catalyst surface and decrease the path length of the photons entering the solution. Therefore, the generation of hydroxyl radicals would be reduced due to the less active sites for hydroxyl anions adsorption and less effective light absorption.

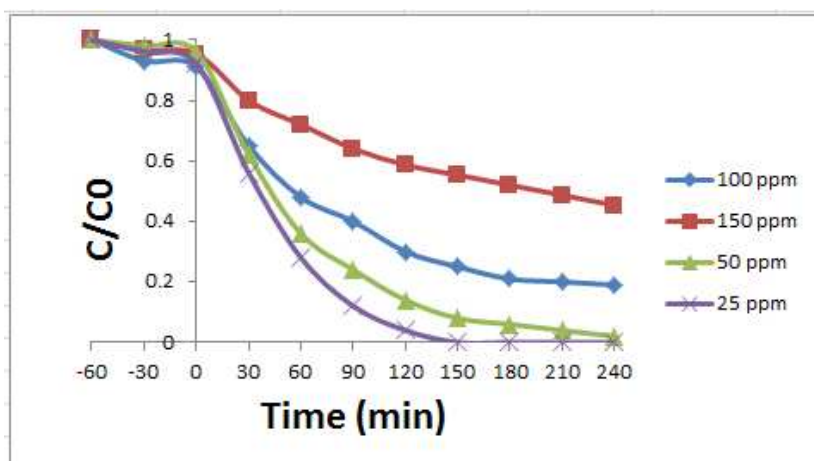


Figure 12. Photocatalytic degradation of phenol using 10%MWCNT/ZnO-Ag (pH=6.8, photocatalyst dosage= 1 gr/L)

- Study of reusability of 10%MWCNT-ZnO-Ag

One of the major drawbacks of ZnO photocatalyst is their severe photo corrosion under light irradiation, which can result in significant decrease of the photocatalytic activity in reused process. The reusability of catalysts is an important factor from economical point of view. Both silver and carbon nanotubes have been reported to be effective in improving the stability of ZnO under light irradiation. In this section, the reusability of 10%MWCNT-ZnO-Ag sample was investigated by evaluating its photocatalytic activity over 10 cycles with the catalyst dosage of 1 g/L and initial concentration of 25 ppm phenol at pH = 6.8 for 150 min. Figure 13 indicates that after 10 successive cycles under UV light, the degradation rate of phenol was 88% for 10%MWCNT-ZnO-Ag sample. It demonstrates that the photo-stability of 10%MWCNT-ZnO-Ag sample is high enough to make the multiple usages possible. The slight decrease in degradation efficiency may be related to the presence of intermediates, which get adsorbed strongly onto the surface of the catalysts and block the active sites. The photocorrosion inhibition of 10%MWCNT-ZnO-Ag could be attributed to the strong interfacial interaction between MWCNTs and ZnO nanoparticles.

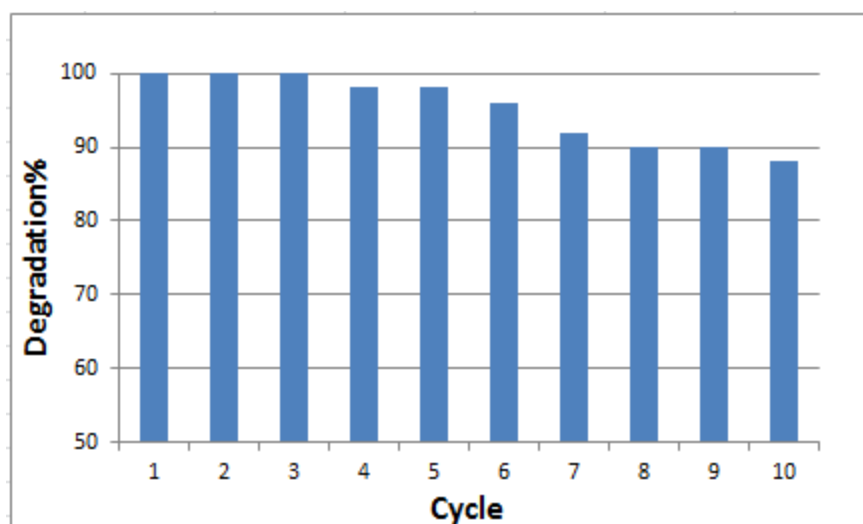


Figure 13. Photocatalytic degradation of phenol over 10%MWCNT/ZnO-Ag after repetitive use

- Photocatalytic mechanism

The photocatalytic process involves many competing reactions. Based on the theory of hetero-structure nanocomposites, we proposed a possible photo degradation mechanism for our hybrid particles, as shown in Fig. 14. When the catalyst surface is exposed to the light with sufficient energy, i.e., equal or larger than band gap, the electron-hole pairs are generated. As the calculated Fermi level of MWCNT is lower than the conduction band edge of ZnO, the photogenerated electrons from ZnO can transfer to the MWCNTs. The high conductive property of CNTs prevents the accumulation of electrons, leads to an effective separation of electron-hole pairs, which is in agreement with PL results. Moreover, Ag and the defects such as oxygen vacancy also act as an electron sink, causing a decrease in the recombination of charge carriers. The photo-induced electron will form the reactive radicals, superoxide radical ion $\cdot\text{O}^{2-}$ and hydroxyl radical $\cdot\text{OH}$, which are responsible for the degradation of the organic compound.(6)

Figure 14. The proposed charge transfer process of MWCNT/ZnO-Ag

- Kinetics of photocatalytic degradation of phenol

The Langmuir-Hinshelwood equation is frequently employed to describe the kinetics of photocatalytic degradation of organic contaminants. This equation is expressed as followings:

$$r = -\frac{dc}{dt} = \frac{k_r K_{ad} C}{1 + K_{ad} C} \quad (2)$$

where, k_r is the reaction rate constant, K_{ad} is the adsorption equilibrium constant of pollutant and t is the irradiation time. When the concentration is low and the adsorption is relatively weak, Eq.(2) can be simplified to the pseudo first order kinetics as followings:

$$\ln(C_0/C) = k_r K_{ad} t = K_{app} t \quad (3)$$

The parameter K_{app} and the half-life of the compound, $t_{1/2}$, can be calculated by plotting $\ln(C_0/C)$ versus time (t). As shown in Fig. 15, the photocatalytic degradation of phenol followed the pseud first order reaction kinetics and the apparent kinetic rate constant, as well as the values of regression coefficient (R^2) are listed in Table 2.

Table 2. Photodegradation rate constant (min^{-1}) and R^2 factor of samples

Sample	K_{app}	R^2
ZnO	0.0029	0.9812
ZnO-Ag	0.0033	0.0514
1%MWCNT/ZnO-Ag	0.0045	0.9617
5%MWCNT/ZnO-Ag	0.0057	0.9877
10%MWCNT/ZnO-Ag	0.0068	0.9497
20%MWCNT/ZnO-Ag	0.0051	0.9862

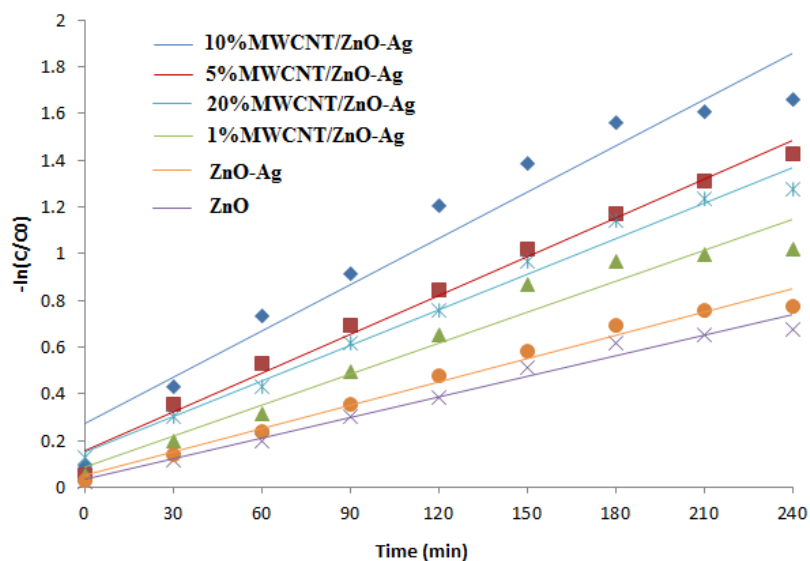


Figure 15. Correlation between experimental data and the Langmuir-Hinshelwood equation

Conclusion

This work reported the synthesis, characterisation and performance of a novel catalytic particle, i.e., Ag-doped ZnO nanoparticle on the support of MWCNTs, in the photocatalytic degradation of phenol. The results showed that the Ag doping caused a band edge shift toward longer wavelength, and the incorporation of MWCNTs enhanced the visible light absorbance and effective separation of electron/hole pair, leading to higher catalytic efficiency. More specific conclusions can be drawn as,

- The MWCNT/ZnO-Ag composites with adjustable MWCNTs concentration can be synthesized easily via the sol-gel method.
- The TEM and SEM study confirmed the Ag doping onto ZnO, and the uniform coverage on CNT surfaces..
- The concentration of MWCNTs affects significantly the recombination rate of photo-generated electron-hole pairs, and there exists an optimum value to achieve the best photocatalytic degradation of phenol. best 81% removal rate for 100 ppm phenol under UVA light after 240 min was obtained by 10%MWCNT/ZnO-Ag sample. .
- The photocatalytic performance was sensitive to pH, catalyst dosage and initial concentration. Phenol degradation percent after 240 min irradiation were 42%, 78%, 81% and 53% respectively at pH 3,5, 6.8 and 11.

- The highest photocatalytic efficiency was obtained at a catalyst dosage of 1 gr/L and an initial concentration of 25 ppm (100% under UVA irradiation for 150 min).
- The 10%MWCNT/ZnO sample can be reused up to 10 cycles without significant loss of catalytic activity, indicating the promising recyclability and photo chemical stability of nanoparticles.
- The kinetics of phenol degradation followed the pseudo-first-order equation.

The synthesized nanocomposites in this work could be utilized as promising cost effective and environmentally friendly materials in the degradation of organic pollutants.

References

- [1] E. Seftel, M. Puscasu, M. Mertens, P. Cool, and G. Carja, "Assemblies of nanoparticles of CeO₂-ZnTi-LDHs and their derived mixed oxides as novel photocatalytic systems for phenol degradation," *Applied Catalysis B: Environmental*, vol. 150, pp. 157-166, 2014.
- [2] E. Grabowska, J. Reszczyńska, and A. Zaleska, "Mechanism of phenol photodegradation in the presence of pure and modified-TiO₂: A review," *Water Research*, vol. 46, pp. 5453-5471, 11/1/ 2012.
- [3] J. Ye, X. Li, J. Hong, J. Chen, and Q. Fan, "Photocatalytic degradation of phenol over ZnO nanosheets immobilized on montmorillonite," *Materials Science in Semiconductor Processing*, vol. 39, pp. 17-22, 11// 2015.

- [4] P. Chowdhury and T. Viraraghavan, "Sonochemical degradation of chlorinated organic compounds, phenolic compounds and organic dyes – A review," *Science of The Total Environment*, vol. 407, pp. 2474-2492, 4/1/ 2009.
- [5] T.-L. Lai, C.-C. Lee, K.-S. Wu, Y.-Y. Shu, and C.-B. Wang, "Microwave-enhanced catalytic degradation of phenol over nickel oxide," *Applied Catalysis B: Environmental*, vol. 68, pp. 147-153, 11/7/ 2006.
- [6] F. Tisa, A. A. Abdul Raman, and W. M. A. Wan Daud, "Applicability of fluidized bed reactor in recalcitrant compound degradation through advanced oxidation processes: A review," *Journal of Environmental Management*, vol. 146, pp. 260-275, 12/15/ 2014.
- [7] A. Fujishima and K. Honda, "Electrochemical Photolysis of Water at a Semiconductor Electrode," *Nature*, vol. 238, pp. 37-38, 07/07/print 1972.
- [8] H. Chun, W. Yizhong, and T. Hongxiao, "Destruction of phenol aqueous solution by photocatalysis or direct photolysis," *Chemosphere*, vol. 41, pp. 1205-9, Oct 2000.
- [9] L. F. Liotta, M. Gruttadauria, G. Di Carlo, G. Perrini, and V. Librando, "Heterogeneous catalytic degradation of phenolic substrates: catalysts activity," *J Hazard Mater*, vol. 162, pp. 588-606, Mar 15 2009.
- [10] M. Nikazar, M. Alizadeh, R. Lalavi, and M. H. Rostami, "The optimum conditions for synthesis of Fe(3)O(4)/ZnO core/shell magnetic nanoparticles for photodegradation of phenol," *Journal of Environmental Health Science and Engineering*, vol. 12, pp. 21-21, 01/09

01/28/received

11/19/accepted 2014.

- [11] R. F. Pontes, J. E. Moraes, A. Machulek, and J. M. Pinto, "A mechanistic kinetic model for phenol degradation by the Fenton process," *Journal of hazardous materials*, vol. 176, pp. 402-413, 2010.
- [12] G. S. Pozan, M. Isleyen, and S. Gokcen, "Transition metal coated TiO₂ nanoparticles: Synthesis, characterization and their photocatalytic activity," *Applied Catalysis B: Environmental*, vol. 140–141, pp. 537-545, 8// 2013.
- [13] J. Prince, F. Tzompantzi, G. Mendoza-Damián, F. Hernández-Beltrán, and J. S. Valente, "Photocatalytic degradation of phenol by semiconducting mixed oxides derived from Zn(Ga)Al layered double hydroxides," *Applied Catalysis B: Environmental*, vol. 163, pp. 352-360, 2// 2015.

- [14] J. S. Valente, F. Tzompantzi, and J. Prince, "Highly efficient photocatalytic elimination of phenol and chlorinated phenols by CeO₂/MgAl layered double hydroxides," *Applied Catalysis B: Environmental*, vol. 102, pp. 276-285, 2011.
- [15] Q. Wang, H. Li, J.-H. Yang, Q. Sun, Q. Li, and J. Yang, "Iron phthalocyanine-graphene donor-acceptor hybrids for visible-light-assisted degradation of phenol in the presence of H₂O₂," *Applied Catalysis B: Environmental*, vol. 192, pp. 182-192, 9/5/ 2016.
- [16] K. Hayat, M. Gondal, M. M. Khaled, S. Ahmed, and A. M. Shemsi, "Nano ZnO synthesis by modified sol gel method and its application in heterogeneous photocatalytic removal of phenol from water," *Applied Catalysis A: General*, vol. 393, pp. 122-129, 2011.
- [17] M. Tobajas, C. Belver, and J. J. Rodriguez, "Degradation of emerging pollutants in water under solar irradiation using novel TiO₂-ZnO/clay nanoarchitectures," *Chemical Engineering Journal*, vol. 309, pp. 596-606, 2/1/ 2017.
- [18] J. Tao, Z. Gong, G. Yao, Y. Cheng, M. Zhang, J. Lv, et al., "Enhanced optical and photocatalytic properties of Ag quantum dots-sensitized nanostructured TiO₂/ZnO heterojunctions," *Journal of Alloys and Compounds*, vol. 688, Part A, pp. 605-612, 12/15/ 2016.
- [19] H. Bel Hadjltaief, M. Ben Zina, M. E. Galvez, and P. Da Costa, "Photocatalytic degradation of methyl green dye in aqueous solution over natural clay-supported ZnO-TiO₂ catalysts," *Journal of Photochemistry and Photobiology A: Chemistry*, vol. 315, pp. 25-33, 1/15/ 2016.
- [20] W. Yu, J. Zhang, and T. Peng, "New insight into the enhanced photocatalytic activity of N-, C- and S-doped ZnO photocatalysts," *Applied Catalysis B: Environmental*, vol. 181, pp. 220-227, 2// 2016.
- [21] Y. Feng, H. Lu, X. Gu, J. Qiu, M. Jia, C. Huang, et al., "ZIF-8 derived porous N-doped ZnO with enhanced visible light-driven photocatalytic activity," *Journal of Physics and Chemistry of Solids*, vol. 102, pp. 110-114, 3// 2017.
- [22] S. Sharma, S. K. Mehta, and S. K. Kansal, "N doped ZnO/C-dots nanoflowers as visible light driven photocatalyst for the degradation of malachite green dye in aqueous phase," *Journal of Alloys and Compounds*, vol. 699, pp. 323-333, 3/30/ 2017.
- [23] S.-W. Zhao, H.-F. Zuo, Y.-R. Guo, and Q.-J. Pan, "Carbon-doped ZnO aided by carboxymethyl cellulose: Fabrication, photoluminescence and photocatalytic applications," *Journal of Alloys and Compounds*, vol. 695, pp. 1029-1037, 2/25/ 2017.

- [24] S. P. Meshram, P. V. Adhyapak, D. P. Amalnerkar, and I. S. Mulla, "Cu doped ZnO microballs as effective sunlight driven photocatalyst," *Ceramics International*, vol. 42, pp. 7482-7489, 5/1/ 2016.
- [25] G. Thennarasu and A. Sivasamy, "Enhanced visible photocatalytic activity of cotton ball like nano structured Cu doped ZnO for the degradation of organic pollutant," *Ecotoxicology and Environmental Safety*, vol. 134, Part 2, pp. 412-420, 12// 2016.
- [26] W. Bousslama, H. Elhouichet, and M. Férid, "Enhanced photocatalytic activity of Fe doped ZnO nanocrystals under sunlight irradiation," *Optik - International Journal for Light and Electron Optics*, vol. 134, pp. 88-98, 4// 2017.
- [27] S. Sood, A. Umar, S. K. Mehta, and S. K. Kansal, "Highly effective Fe-doped TiO₂ nanoparticles photocatalysts for visible-light driven photocatalytic degradation of toxic organic compounds," *Journal of Colloid and Interface Science*, vol. 450, pp. 213-223, 7/15/ 2015.
- [28] A. Šutka, T. Käämbre, R. Pärna, I. Juhneviča, M. Maiorov, U. Joost, et al., "Co doped ZnO nanowires as visible light photocatalysts," *Solid State Sciences*, vol. 56, pp. 54-62, 6// 2016.
- [29] C. A. Gouvea, F. Wypych, S. G. Moraes, N. Duran, N. Nagata, and P. Peralta-Zamora, "Semiconductor-assisted photocatalytic degradation of reactive dyes in aqueous solution," *Chemosphere*, vol. 40, pp. 433-40, Feb 2000.
- [30] H. Bouzid, M. Faisal, F. A. Harraz, S. A. Al-Sayari, and A. A. Ismail, "Synthesis of mesoporous Ag/ZnO nanocrystals with enhanced photocatalytic activity," *Catalysis Today*, vol. 252, pp. 20-26, 9/1/ 2015.
- [31] S. Mohammadzadeh, M. E. Olya, A. M. Arabi, A. Shariati, and M. R. Khosravi Nikou, "Synthesis, characterization and application of ZnO-Ag as a nanophotocatalyst for organic compounds degradation, mechanism and economic study," *Journal of Environmental Sciences*, vol. 35, pp. 194-207, 9/1/ 2015.
- [32] M. Faisal, H. Bouzid, F. A. Harraz, A. A. Ismail, S. A. Al-Sayari, and M. S. Al-Assiri, "Mesoporous Ag/ZnO multilayer films prepared by repeated spin-coating for enhancing its photonic efficiencies," *Surface and Coatings Technology*, vol. 263, pp. 44-53, 2/15/ 2015.
- [33] J. b. Zhong, J. z. Li, X. y. He, J. Zeng, Y. Lu, W. Hu, et al., "Improved photocatalytic performance of Pd-doped ZnO," *Current Applied Physics*, vol. 12, pp. 998-1001, 5// 2012.

- [34] N. Güy, S. Çakar, and M. Özacar, "Comparison of palladium/zinc oxide photocatalysts prepared by different palladium doping methods for congo red degradation," *Journal of Colloid and Interface Science*, vol. 466, pp. 128-137, 3/15/ 2016.
- [35] P. K. Chen, G. J. Lee, S. H. Davies, S. J. Masten, R. Amutha, and J. J. Wu, "Hydrothermal synthesis of coral-like Au/ZnO catalyst and photocatalytic degradation of Orange II dye," *Materials Research Bulletin*, vol. 48, pp. 2375-2382, 6// 2013.
- [36] N. Morales-Flores, U. Pal, and E. Sánchez Mora, "Photocatalytic behavior of ZnO and Pt-incorporated ZnO nanoparticles in phenol degradation," *Applied Catalysis A: General*, vol. 394, pp. 269-275, 2/28/ 2011.
- [37] T.-J. Whang, M.-T. Hsieh, and H.-H. Chen, "Visible-light photocatalytic degradation of methylene blue with laser-induced Ag/ZnO nanoparticles," *Applied Surface Science*, vol. 258, pp. 2796-2801, 1/15/ 2012.
- [38] B. Divband, M. Khatamian, G. R. K. Eslamian, and M. Darbandi, "Synthesis of Ag/ZnO nanostructures by different methods and investigation of their photocatalytic efficiency for 4-nitrophenol degradation," *Applied Surface Science*, vol. 284, pp. 80-86, 11/1/ 2013.
- [39] M. J. Height, S. E. Pratsinis, O. Mekasuwandumrong, and P. Praserthdam, "Ag-ZnO catalysts for UV-photodegradation of methylene blue," *Applied Catalysis B: Environmental*, vol. 63, pp. 305-312, 3/31/ 2006.
- [40] S. George, S. Pokhrel, Z. Ji, B. L. Henderson, T. Xia, L. Li, et al., "Role of Fe doping in tuning the band gap of TiO₂ for photo-oxidation induced cytotoxicity paradigm," *Journal of the American Chemical Society*, vol. 133, pp. 11270-11278, 07/01 2011.
- [41] V. Subramanian, E. Wolf, and P. V. Kamat, "Semiconductor– Metal Composite Nanostructures. To What Extent Do Metal Nanoparticles Improve the Photocatalytic Activity of TiO₂ Films?," *The Journal of Physical Chemistry B*, vol. 105, pp. 11439-11446, 2001.
- [42] S. T. Kochuveedu, Y. H. Jang, and D. H. Kim, "A study on the mechanism for the interaction of light with noble metal-metal oxide semiconductor nanostructures for various photophysical applications," *Chemical Society Reviews*, vol. 42, pp. 8467-8493, 2013.
- [43] S. A. Ansari, M. M. Khan, M. O. Ansari, J. Lee, and M. H. Cho, "Biogenic Synthesis, Photocatalytic, and Photoelectrochemical Performance of Ag–ZnO Nanocomposite," *The Journal of Physical Chemistry C*, vol. 117, pp. 27023-27030, 2013/12/27 2013.

- [44] Z. Han, L. Ren, Z. Cui, C. Chen, H. Pan, and J. Chen, "Ag/ZnO flower heterostructures as a visible-light driven photocatalyst via surface plasmon resonance," *Applied Catalysis B: Environmental*, vol. 126, pp. 298-305, 9/25/ 2012.
- [45] Y. Yan, M. Al-Jassim, and S.-H. Wei, "Doping of ZnO by group-IB elements," *Applied physics letters*, vol. 89, p. 181912, 2006.
- [46] Y. Ma, G. Du, S. Yang, Z. Li, B. Zhao, X. Yang, et al., "Control of conductivity type in undoped ZnO thin films grown by metalorganic vapor phase epitaxy," *Journal of applied physics*, vol. 95, pp. 6268-6272, 2004.
- [47] M. A. Thomas, W. W. Sun, and J. B. Cui, "Mechanism of Ag Doping in ZnO Nanowires by Electrodeposition: Experimental and Theoretical Insights," *The Journal of Physical Chemistry C*, vol. 116, pp. 6383-6391, 2012/03/15 2012.
- [48] O. Lupan, L. Chow, L. K. Ono, B. R. Cuenya, G. Chai, H. Khallaf, et al., "Synthesis and Characterization of Ag- or Sb-Doped ZnO Nanorods by a Facile Hydrothermal Route," *The Journal of Physical Chemistry C*, vol. 114, pp. 12401-12408, 2010/07/29 2010.
- [49] S. M. Hosseini, I. A. Sarsari, P. Kameli, and H. Salamati, "Effect of Ag doping on structural, optical, and photocatalytic properties of ZnO nanoparticles," *Journal of Alloys and Compounds*, vol. 640, pp. 408-415, 8/15/ 2015.
- [50] Z. Q. He, D. Wang, H. Y. Fang, J. M. Chen, and S. Song, "Highly efficient and stable Ag/AgIO₃ particles for photocatalytic reduction of CO₂ under visible light," *Nanoscale*, vol. 6, pp. 10540-10544, 2014.
- [51] T. Liu, B. Li, Y. Hao, F. Han, L. Zhang, and L. Hu, "A general method to diverse silver/mesoporous-metal-oxide nanocomposites with plasmon-enhanced photocatalytic activity," *Applied Catalysis B: Environmental*, vol. 165, pp. 378-388, 4// 2015.
- [52] M. Rycenga, C. M. Cobley, J. Zeng, W. Li, C. H. Moran, Q. Zhang, et al., "Controlling the synthesis and assembly of silver nanostructures for plasmonic applications," *Chem Rev*, vol. 111, pp. 3669-712, Jun 08 2011.
- [53] S. Linic, P. Christopher, H. Xin, and A. Marimuthu, "Catalytic and Photocatalytic Transformations on Metal Nanoparticles with Targeted Geometric and Plasmonic Properties," *Accounts of Chemical Research*, vol. 46, pp. 1890-1899, 2013/08/20 2013.
- [54] S. V. Boriskina, H. Ghasemi, and G. Chen, "Plasmonic materials for energy: From physics to applications," *Materials Today*, vol. 16, pp. 375-386, 10// 2013.

- [55] M. Khademalrasool, M. Farbod, and A. Irajizad, "Preparation of ZnO nanoparticles/Ag nanowires nanocomposites as plasmonic photocatalysts and investigation of the effect of concentration and diameter size of Ag nanowires on their photocatalytic performance," *Journal of Alloys and Compounds*, vol. 664, pp. 707-714, 4/15/ 2016.
- [56] R. H. Baughman, A. A. Zakhidov, and W. A. de Heer, "Carbon nanotubes--the route toward applications," *Science*, vol. 297, pp. 787-92, Aug 02 2002.
- [57] B. Li and H. Cao, "ZnO@graphene composite with enhanced performance for the removal of dye from water," *Journal of Materials Chemistry*, vol. 21, pp. 3346-3349, 2011.
- [58] S. J. Tans, A. R. M. Verschueren, and C. Dekker, "Room-temperature transistor based on a single carbon nanotube," *Nature*, vol. 393, pp. 49-52, 05/07/print 1998.
- [59] C. S. Chen, T. G. Liu, L. W. Lin, X. D. Xie, X. H. Chen, Q. C. Liu, et al., "Multi-walled carbon nanotube-supported metal-doped ZnO nanoparticles and their photocatalytic property," *Journal of Nanoparticle Research*, vol. 15, p. 1295, 12/16

07/20/received

11/08/accepted 2013.

- [60] Y. Yu, J. C. Yu, J.-G. Yu, Y.-C. Kwok, Y.-K. Che, J.-C. Zhao, et al., "Enhancement of photocatalytic activity of mesoporous TiO₂ by using carbon nanotubes," *Applied Catalysis A: General*, vol. 289, pp. 186-196, 8/10/ 2005.
- [61] T. A. Saleh, M. A. Gondal, and Q. A. Drmoseh, "Preparation of a MWCNT/ZnO nanocomposite and its photocatalytic activity for the removal of cyanide from water using a laser," *Nanotechnology*, vol. 21, p. 495705, Dec 10 2010.
- [62] K. Byrappa, A. S. Dayananda, C. P. Sajan, B. Basavalingu, M. B. Shayan, K. Soga, et al., "Hydrothermal preparation of ZnO:CNT and TiO₂:CNT composites and their photocatalytic applications," *Journal of Materials Science*, vol. 43, pp. 2348-2355, 2008// 2008.
- [63] C. Martínez, M. Canle L, M. I. Fernández, J. A. Santaballa, and J. Faria, "Kinetics and mechanism of aqueous degradation of carbamazepine by heterogeneous photocatalysis using nanocrystalline TiO₂, ZnO and multi-walled carbon nanotubes--anatase composites," *Applied Catalysis B: Environmental*, vol. 102, pp. 563-571, 2/22/ 2011.

- [64] L. Jiang and L. Gao, "Fabrication and characterization of ZnO-coated multi-walled carbon nanotubes with enhanced photocatalytic activity," *Materials Chemistry and Physics*, vol. 91, pp. 313-316, 6/15/ 2005.
- [65] I. Y. Y. Bu, "Optoelectronic properties of solution synthesis of carbon nanotube/ZnO:Al:N nanocomposite and its potential as a photocatalyst," *Materials Science in Semiconductor Processing*, vol. 22, pp. 76-82, 6// 2014.